

REVIEW ARTICLE

Gold nanoparticles: Optical properties and implementations in cancer diagnosis and photothermal therapy

Xiaohua Huang ^{a,b}, Mostafa A. El-Sayed ^{a,*}

^a *Laser Dynamics Laboratory, School of Chemistry and Biochemistry, Georgia Institute of Technology, Atlanta, GA 30332-0400, USA*

^b *Emory-Georgia Tech Cancer Center for Nanotechnology Excellence, Department of Biomedical Engineering, Emory University and Georgia Institute of Technology, Atlanta, GA 30322, USA*

KEYWORDS

Gold nanoparticles;
Cancer;
Imaging;
Photothermal therapy

Abstract Currently a popular area in nanomedicine is the implementation of plasmonic gold nanoparticles for cancer diagnosis and photothermal therapy, attributed to the intriguing optical properties of the nanoparticles. The surface plasmon resonance, a unique phenomenon to plasmonic (noble metal) nanoparticles leads to strong electromagnetic fields on the particle surface and consequently enhances all the radiative properties such as absorption and scattering. Additionally, the strongly absorbed light is converted to heat quickly via a series of nonradiative processes. In this review, we discuss these important optical and photothermal properties of gold nanoparticles in different shapes and structures and address their recent applications for cancer imaging, spectroscopic detection and photothermal therapy.

© 2009 University of Cairo. All rights reserved.

Introduction

Nanomedicine is currently an active field. This is because new properties emerge when the size of a matter is reduced from bulk to the nanometer scale [1,2]. These new properties, including optical, magnetic, electronic, and structural properties, make nano-sized particles (generally 1–100 nm) very promising

for a wide range of biomedical applications such as cellular imaging, molecular diagnosis and targeted therapy depending on the structure, composite and shape of the nanomaterials [3]. Plasmonic (noble metal) nanoparticles distinguish themselves from other nanoplatforms such as semiconductor quantum dots, magnetic and polymeric nanoparticle by their unique surface plasmon resonance (SPR). This SPR, resulting from photon confinement to a small particle size, enhances all the radiative and nonradiative properties of the nanoparticles [4–6] and thus offering multiple modalities for biological and medical applications [7–12].

Gold nanoparticles (Au NPs) have been brought to the forefront of cancer research in recent years because of their facile synthesis and surface modification, strongly enhanced and tunable optical properties as well as excellent biocompatibility feasible for clinic settings. High quality, high yield and size controllable colloidal gold can be quickly prepared by

* Corresponding author. Tel.: +1 404 894 0292; fax: +1 404 894 0294.
E-mail address: melsayed@gatech.edu (M.A. El-Sayed).

2090-1232 © 2009 University of Cairo. All rights reserved. Peer review under responsibility of University of Cairo.



the well-known citrate reduction method [13–15]. Synthetic advancement in the last decade engenders Au NPs of different shapes and structure [16] including gold nanorods [17–19], silica/gold nanoshells [20] and hollow Au NPs [21], which all show largely red-shifted properties boosting their values in photothermal cancer therapy [22–24]. The strongly enhanced radiative properties such as absorption, scattering and plasmonic field for surface enhanced Raman of adjacent molecules make them extremely useful for molecular cancer imaging [23,25–28].

In this review, we will introduce the optical and photothermal properties of Au NPs in different shapes and structures starting with the elucidation of surface plasmon resonance. Their biomedical applications in cancer imaging using light scattering properties, spectroscopic cancer detection using surface enhanced Raman and photothermal therapy using nonradiative properties will be summarized and discussed.

Surface plasmon resonance

The enchantment of Au NPs since ancient times, as reflected in their intense color, originates from the basic photophysical response that does not exist to nonmetallic particles. When a metal particle is exposed to light, the oscillating electromagnetic field of the light induces a collective coherent oscillation of the free electrons (conduction band electrons) of the metal. This electron oscillation around the particle surface causes a charge separation with respect to the ionic lattice, forming a

dipole oscillation along the direction of the electric field of the light (Fig. 1A). The amplitude of the oscillation reaches maximum at a specific frequency, called surface plasmon resonance (SPR) [29–33]. The SPR induces a strong absorption of the incident light and thus can be measured using a UV–Vis absorption spectrometer. The SPR band is much stronger for plasmonic nanoparticles (noble metal, especially Au and Ag) than other metals. The SPR band intensity and wavelength depends on the factors affecting the electron charge density on the particle surface such as the metal type, particle size, shape, structure, composition and the dielectric constant of the surrounding medium, as theoretically described by Mie theory [29]. For particles smaller than 20 nm, the SPR can be quantitatively explained according to the following simple equation [4–6,8,29–34].

$$C_{\text{ext}} = \frac{24\pi^2 R^3 \epsilon_m^{3/2}}{\lambda} \frac{\epsilon_i}{(\epsilon_r + 2\epsilon_m)^2 + \epsilon_i^2} \quad (1)$$

where C_{ext} is the extinction cross-section which is related to extinction coefficient by ϵ ($M^{-1} cm^{-1}$) = $10^{-3} N_0 C_{\text{ext}}(cm^2)/2.303$, λ is the wavelength of the incident light, ϵ is the complex dielectric constant of the metal given by $\epsilon = \epsilon_r(\omega) + i\epsilon_i(\omega)$, $\epsilon_r(\omega)$ is the real part and $\epsilon_i(\omega)$ is the imagery part of the dielectric function of the metal, ϵ_m is the dielectric constant of the surrounding medium which is related to the refractive index of the medium by $\epsilon_m = n_m^2$. The real part of the dielectric constant of the metal determines the SPR position and the imagery part determines the bandwidth. The SPR resonance occurs

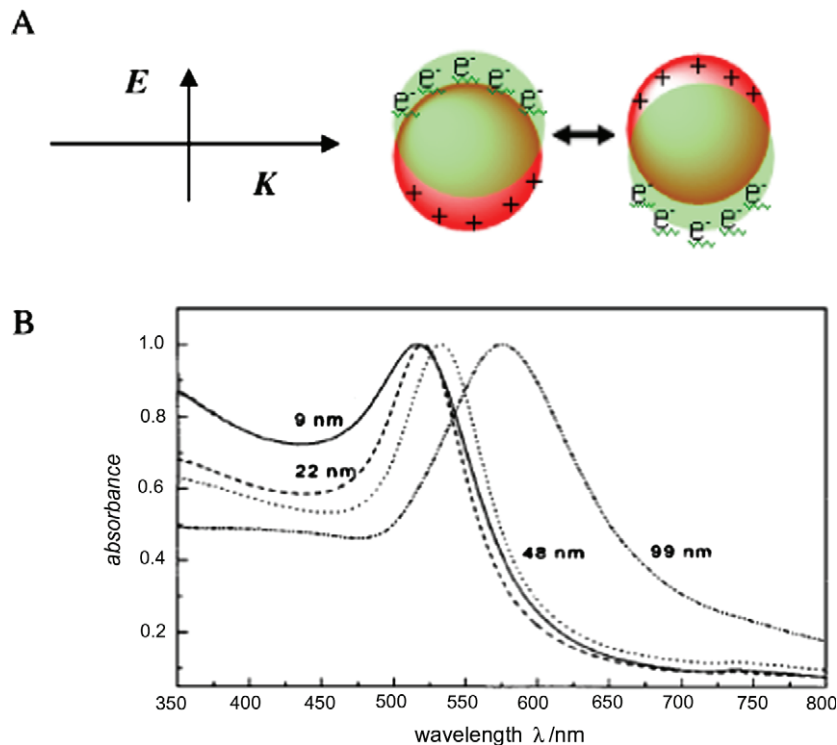


Figure 1 (A). Schematic illustration of surface plasmon resonance in plasmonic nanoparticles. (B). Extinction spectra of gold nanoparticles in different sizes. The electric field of incident light induces coherent collective oscillation of conduction band electrons with respect to the positively charged metallic core. This dipolar oscillation is resonant with the incoming light at a specific frequency that depends on particle size and shape. For gold nanoparticles, the SPR wavelength is around 520 nm depending on the size of the nanoparticles ((B) is reproduced with permission from Ref. [37]).

when $\varepsilon_r(\omega) = -2\varepsilon_m$. Gold, silver and copper nanoparticles show strong SPR bands in the visible region while other metals show broad and weak band in the UV region [35,36].

Au NPs show the SPR band around 520 nm in the visible region. The SPR band is affected by the particle size [37] (Fig. 1B). The SPR band of Au NPs with size smaller than 10 nm is largely damped due to the phase changes resulting from the increased rate of electron-surface collisions compared to larger particles [38,39]. Increasing particle size red shifts the SPR wavelength and also increases the intensity. For particles larger than 100 nm, the band broadening is obvious due to the dominate contributions from higher order electron oscillations.

Surface plasmon absorption and scattering

The energy loss of electromagnetic wave (total light extinction) after passing through a matter results from two contributions: absorption and scattering processes. Light absorption results when the photon energy is dissipated due to inelastic processes. Light scattering occurs when the photon energy causes electron oscillations in the matter which emit photons in the form of scattered light either at the same frequency as the incident light (Rayleigh scattering) or at a shifted frequency (Raman scattering). The frequency shift corresponds to the energy difference created molecular motion within the matter (molecular bond rotations, stretching or vibrations). Due to the SPR oscillation, the light absorption and scattering are strongly enhanced, 5–6 orders of magnitude stronger than most strongly absorbing organic dye molecules and than the emission of most strongly fluorescent molecules, respectively [40].

The surface plasmon absorption, scattering and total extinction efficiencies are generally studied by using full Mie

theory [29]. This is because for nanoparticles larger than 20 nm, higher order electron oscillations start to take important roles and the light absorption and scattering are described by considering all multiple oscillations [33]. As shown from the calculated results by El-Sayed and co-workers using full Mie theory [40,41], the optical absorption and scattering is largely dependent on the size of the nanoparticles. For a 20 nm Au NP, the total extinction is nearly all contributed by absorption [40] (Fig. 2A). When the size increases to 40 nm, the scattering starts to show up (Fig. 2B). When the size increases to 80 nm, the extinction is contributed by both absorption and scattering in a similar degree (Fig. 2C). From the quantitative relationship (Fig. 2D), it can be seen that the ratio of the scattering to absorption increases dramatically for larger size of particles. This fact can guide the choice of gold nanoparticles for biomedical applications. For imaging, lager nanoparticles are preferred because of higher scattering efficiency, whereas for photothermal therapy, smaller nanoparticles are preferred as light is mainly adsorbed by the particles and thus efficiently converted to heat for cell and tissue destruction.

Optical tuning by shape and structure

Gold nanorods

Au NPs have fantasized scientist for decades largely due to the ability of optical tuning by synthetic controlling of the particle shape, composition and structure. As predicted by Gan theory in 1915 [42], when the shape of Au NPs change from spheres to rods (Fig. 3A), the SPR band is split into two bands: a strong band in NIR region corresponding to electron oscillations along the long axis, referred to longitudinal band, and a weak band in the visible region at a wavelength similar to that of gold

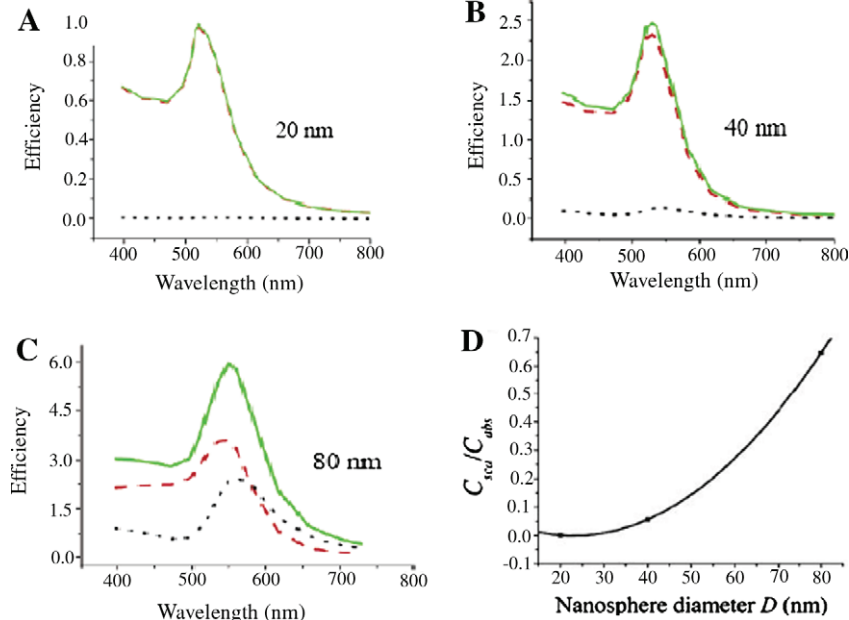


Figure 2 Tuning of the relative contribution of surface plasmon absorption and scattering by changing the particle size. The calculated surface plasmon absorption, scattering and total extinction efficiencies of gold nanoparticles in diameter of (A) 20 nm; (B) 40 nm and (C) 80 nm. (D) The dependence of the ratio of the scattering to absorption cross-sections to on the diameter of gold nanoparticles. Increase particle sizes lead to increased contribution from Mie scattering. The calculations are made by using full Mie theory. (Reproduced with permission from Ref. [40].)

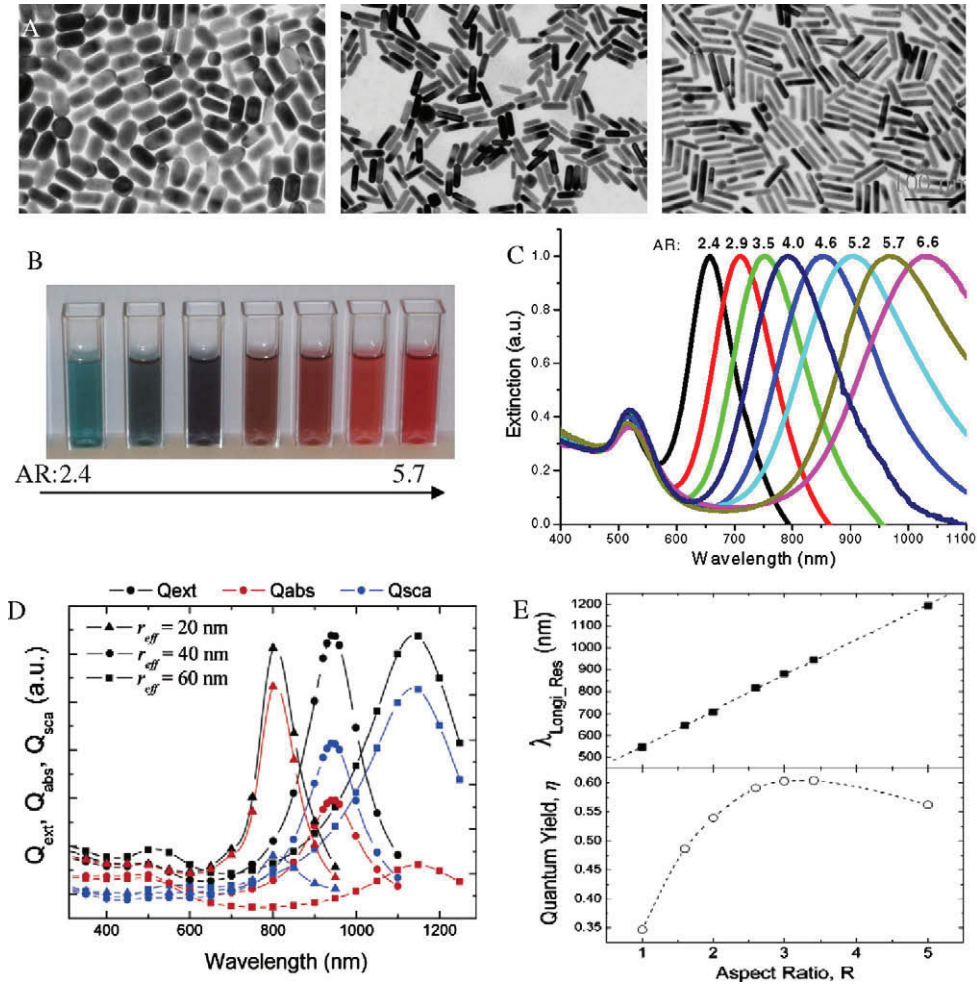


Figure 3 Tunable optical properties of gold nanorods by changing the aspect ratios. Gold nanorods of different aspect ratios exhibit different dimensions as seen by TEM (A), in different color (B) and different SPR wavelength (C). (D) DDA simulation of the optical properties of gold nanorods of different hydrodynamic diameters. (E) The dependence of SPR wavelength on the aspect ratio (top) and the dependence of scattering quantum yield (scattering efficiency/absorption efficiency) on the aspect ratio (bottom) ((D) and (E) are reproduced with permission from Ref. [41]).

nanospheres, referred to transverse bands. While the transverse band is insensitive to the size changes, the longitudinal band is red shifted largely from the visible to near-infrared region with increasing aspect ratios (Length/Width), causing the color changes from blue to red (Fig. 3B and C). Currently, the aspect ratio can be precisely controlled by changing the experimental parameters such as the catalyst of silver ions in the seed-mediated growth method developed by Murphy and El-Sayed groups [18,19]. The nanorods are formed by asymmetric growth of small gold spheres in the presence of shape-forming surfactants, weak reducing agents and the catalysts [43].

According to Gan theory, the extinction coefficient γ can be quantitatively expressed as [44]:

$$\gamma = \frac{2\pi N V \epsilon_m^{3/2}}{3\lambda} \sum_j \frac{(1/P_j^2)\epsilon_2}{\left(\epsilon_1 + \frac{1-P_j}{P_j}\epsilon_m\right)^2 + \epsilon_2^2} \quad (2)$$

where N is the number of particles per unit volume, V is the volume of each particle, λ is the wavelength of the incident light, ϵ is the complex dielectric constant of the metal given by $\epsilon = \epsilon_r$

$(\omega) + i\epsilon_i(\omega)$, $\epsilon_r(\omega)$ is the real part and $\epsilon_i(\omega)$ is the imagery part of the dielectric constant of the metal, respectively, ϵ_m is the dielectric constant of the surrounding medium, P_j is defined as

$$P_A = \frac{1-e^2}{e^2} \left[\frac{1}{2e} \ln \left(\frac{1+e}{1-e} \right) - 1 \right] \quad (3)$$

$$P_B = P_C = \frac{1-P_A}{2} \quad (4)$$

where

$$e = \sqrt{1 - \left(\frac{B}{A} \right)^2} \quad (5)$$

A , B and C are the three axes of the rods with $A > B = C$. The A/B is the aspect ratio. The resonance occurs at $\epsilon_1 = -(1 - P_j^{(i)})\epsilon_m/P_j^{(i)}$ where $i = A$ for longitudinal resonance and $i = B, C$ for transverse resonance.

Bases on Eq. (2) and the relationship of the real part of the dielectric constant of gold with light wavelength in the form of $\epsilon_r(\omega) = 34.66 - 0.07\lambda$, Link and El-Sayed [44,45] found a linear proportional relationship between the longitudinal SPR

absorption maximum and the aspect ratio of nanorods in the aqueous solution:

$$\lambda_{max} = 95R + 420 \quad (6)$$

As the aspect ratio increases, the SPR maximum is linearly red shifted. Such optical behavior is totally different from spheres for which the SPR only slightly red shifts with increasing the particle size.

Gan theory is developed for short rods with cylinder shape as it only considers dipole oscillations. For nanorods with any aspect ratios, discrete dipole approximation (DDA), a powerful electrodynamics and numerical methods to calculate optical properties of targets with any arbitrary geometry and composition [46–50] is generally used. In this numerical method, the target particle is viewed as a cubic array of point dipoles. Each dipole interacts with the electric field of incident light and the induced field by other dipoles. From the dipole moment with an initial guess, the extinction, absorption and scattering cross-sections can be derived from the optical theorem.

DDA provides an easy way to analyze the effects of the size and geometry on the SPR absorption, scattering and total extinction. El-Sayed and co-workers adopted DDA and studied the optical properties of gold nanorods in different hydrodynamic size [51]. When the aspect ratio increases, light scattering efficiency greatly increases (Fig. 3D). As predicted by Gan theory, the absorption wavelength is linearly dependent on the aspect ratios (Fig. 3E, top). Similar to gold nanospheres, when the aspect ratios increase, the scattering

efficiency increases (Fig. 3E, bottom). The ratio of scattering efficiency (Q_{sca}) to the total extinction efficiency (Q_{ext}) at their respective resonance maximum, defined as scattering quantum yield, increases dramatically with increasing the aspect ratio but drops slightly with further increase in the elongation with a turning aspect ratio at 3.4 for the rods with the same effective radius of 40 nm. The drop of the quantum yield is due to the increases in the absorption efficiency at higher aspect ratios resulting from the increases of the imaginary part of the dielectric constant of the metal. They also found out that the scattering quantum yield is enhanced from 0.326 for a sphere to 0.603 for a rod by only elongating the shape.

Gold nanoshell and gold nanocage

Besides the shape factor for optical tuning into NIR region, structure variation can results in similar phenomenon. Two examples are the gold nanoshells and nanocages (Fig. 4). Developed by Halas and co-workers [20], gold nanoshell is composed of a silica core around 100 nm and a thin shell of gold about few nanometers. The shell is formed by aging the gold clusters attached on the silicon core. The red shift has been explained as the results of the hybridization of the plasmons of the inner sphere and outer cavity [52]. The SPR wavelength of gold nanoshells can be controlled by changing the shell thickness. Decreasing the thickness of the gold shell from 20 to 5 nm leads to SPR red shift about 300 nm, which is attributed to the increased coupling between the inner and outer shell surface plasmons for

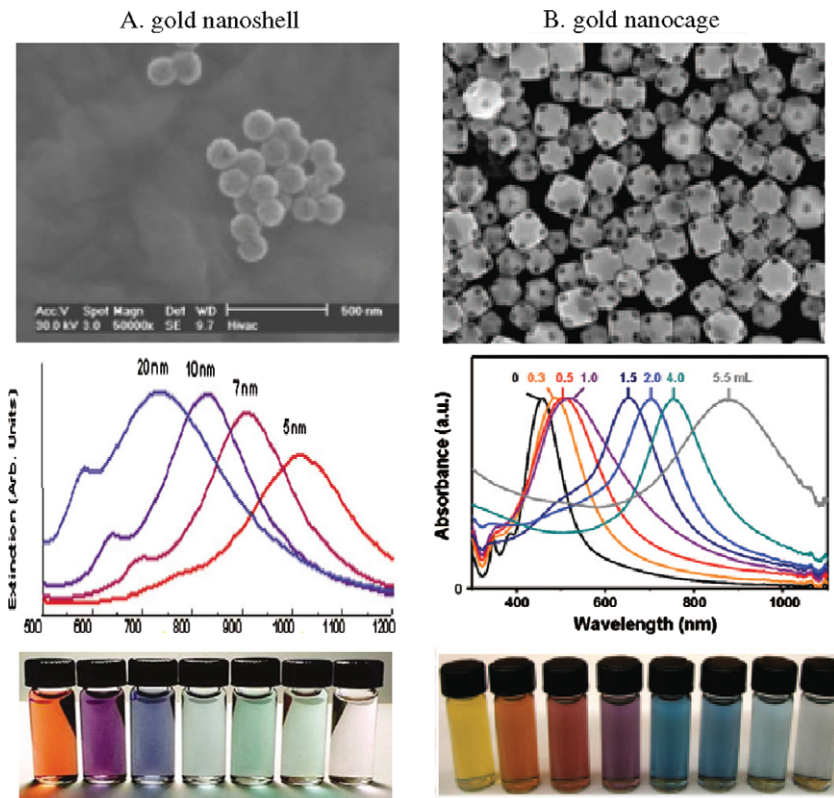


Figure 4 Tunable optical properties of gold nanoshells by changing the shell thickness (A) and gold nanocages by changing the auric acid in the synthetic procedure (B). Top row: TEM; middle row: absorption spectra; bottom row: physical appearance ((A) is reproduced with permission from Ref. [27]. (B) is reproduced with permission from Ref. [12]).

thinner shell particles [52]. Recently, DDA simulation shows that the SPR frequency depends on the ratio of the shell-to-core thickness in a near-exponential relationship which is independent of the particle size, core and shell material and even surrounding medium [53].

Developed lately by Xia and co-workers [21], gold nanocages are a type of hollow and porous gold nanostructures which are formed by a galvanic replacement reaction between silver nanocubes and auric acid in aqueous solution. Simultaneous deposition of gold atoms and depletion of silver atoms results in gold nanoshells which then anneal to generate smooth hollow and porous structures. General size of the nanocages is around 50 nm edge width with few nanometers walls and holes for SPR wavelength around 800 nm [54]. By controlling the amount of auric acid solution, the SPR of gold nanocages could be tuned to NIR region with specified wavelength. DDA calculation [55] shows that the total light extinction of gold nanocages with SPR around 800 nm is dominated by absorption, which makes them suitable for photothermal therapy.

Nonradiative properties

In addition to the enhanced and tunable radiative properties mainly light scattering useful for optical imaging, Au NPs can convert the absorbed light into heat via a series of nonradiative processes, which have been extensively studied by El-Sayed group and some other workers using ultrafast dynamics [2,4–6,56–60]. Basically, the energy transformation process starts by the fast phase loss of the coherently excited electrons (on femtoseconds) via electron–electron collisions leading hot electrons with temperatures as high as 1000 K. Then the electron passes the energy to the phonon by electron–phonon interactions on the order of 0.5–1 ps, resulting in a hot lattice with temperature rises on the order of a few tens of degrees. The electron–phonon relaxation process is size and shape independent and also independent for both the transverse or longitudinal surface plasmon in the rods [61].

Depending on the hot energy content, three subsequent processes can occur: (1) The lattice cools off by passing its heat to the surrounding medium via phonon–phonon relaxation within \sim 100 ps. This process leads to the heat-up of the surrounding medium. Such fast energy conversion and dissipation can be utilized for sufficient heating of physically adsorbed or chemically attached cancer cells by using a selected wavelength of light that overlaps maximally with the nanoparticle SPR absorption band. (2) The lattice heat content is sufficient enough to lead to particle melting. The lattice heating by the electrons and cooling by surrounding medium is a competitive process. If the heating rate is much faster than the cooling rate, massive heat is accumulated within the lattice sufficient enough to lead to particle structural changes such as nanoparticle melting or fragmentation in nanoseconds. In 1999, Link et al. [61,62] found that nanorods melted into near spherical particles of comparable volumes at moderate energies using a 100-fs laser at 800 nm while fragmented into smaller spheres when using a high energy 7-ns laser or higher energy of fs laser. (3) The lattice heat content is sufficient enough to result in particle ablation in hundreds of femtoseconds. In order to use the produced heat for the cure of cancer, the first process has to be dominated which is generally realized by using continuous

wave lasers to allow heat dissipation from particles to surrounding medium. High energy pulsed laser generally lead to particle structure changes and ablation due to rapid massive heat creation with the high intensity laser pulses in a very short time.

Cancer imaging

As shown in the previous section, Au NPs scatter strongly and the scattering properties depend on the size, shape and structure of the nanoparticles [40,41,51,63–68]. Typically, nanoparticles of 30–100 nm diameter scatter intensely and can be detected easily by a commercial microscope under dark-field illumination conditions [67]. In fact, 40 nm An NPs can be easily detected by eye down to a particle concentration of 10^{-14} M [63,64]. Likewise, the scattering from a 60 nm An NPs is 10^5 stronger than the emission of a fluorescein molecule [40,64]. Similarly, a 70 nm An NPs scatter orders of magnitude stronger than that of a polystyrene sphere in the same size (Fig. 5A and B) [25]. The high scattering cross-sections of An NPs together with their superior photostability (as compared to organic dyes) make them extremely promising for cellular imaging [23,25–28,69–78].

The feasibility of An NPs for cancer imaging has been demonstrated in recent years [23,25–28,75]. In the earlier attempts by Sokolov et al., the scattered light is collected in a reflection mode under single laser wavelength excitation using a confocal microscope or simply a laser pen [25,26]. In these work, An NPs are conjugated to anti-epidermal growth factor receptor (anti-EGFR) antibodies via nonspecific adsorption to recognize the EGFR proteins on the cervical carcinoma cells and tissues. Compared to the cancer cells treated with BSA-adsorbed nanoparticles, those incubated with the targeted particles scatter strongly due to the bound nanoparticles on the membrane of the cancer cells (Fig. 5C and D). On the tissue level, the strongly scattered signals enable the detection of abnormal tissues in contrast to weak auto-scattering from normal tissue (Fig. 5E and F).

An improvement of the cancer imaging based on the scattering properties of An NPs was made by El-Sayed et al. using dark field microscopy in 2005 [28]. In this case, the nanoparticles are excited by the white light from a halogen lamp which is also the same lamp used for bright field imaging. In the dark field (Fig. 6A and B), a dark field condenser delivers and focuses a very narrow beam of white light on the top of the sample with the center illumination light blocked by the aperture. The objective with an iris for adjusting light collection zone is used to collect only the scattered light from the samples and thus presents an image of bright object in a dark background. As the nanoparticles scatter light most strongly at the wavelength of the SPR maximum, the nanoparticles appears in brilliant color that depends on the size and shape of the particles. As a matter of fact, the dark field light scattering imaging of individual An NPs was made much earlier back in 1914 by Zsigmondy using an ultra-microscope [79]. Comparatively, a similar dark field imaging was developed by Yguerabide et al. in 1998 to image An NPs in solution with a side illumination mode [63,64]. The light is delivered to the sample with an angled position by a flexible optic fiber light guide and the scattered light is collected by the objective of the optical microscope [64]. However, this self-built setup requires extensive

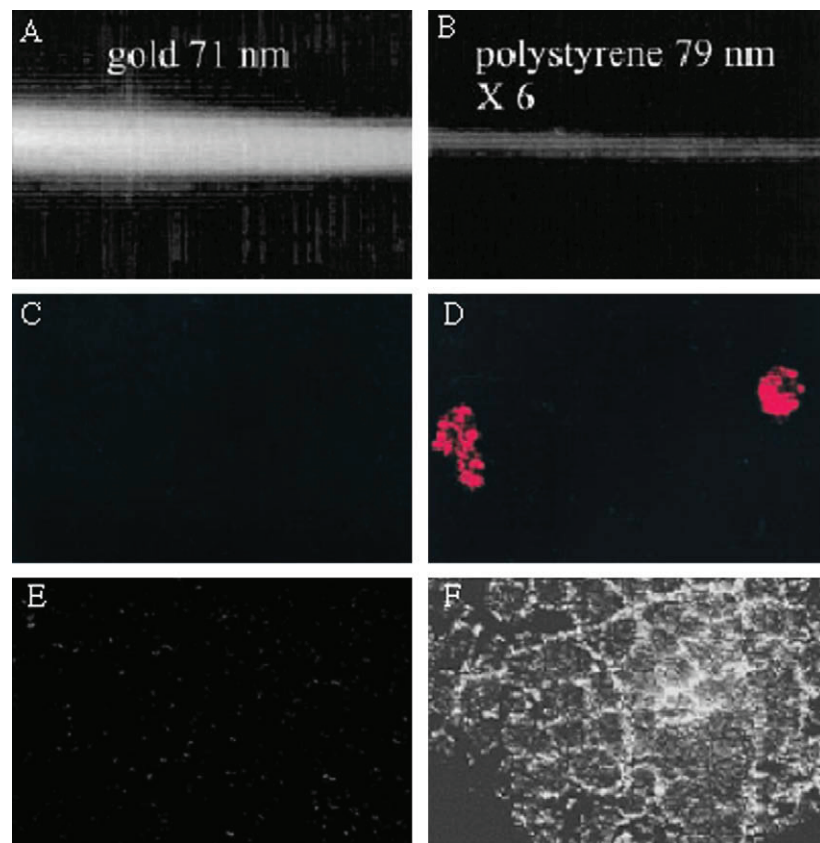


Figure 5 (A and B) Comparison of scattering properties of gold nanoparticles (A) and polystyrene nanoparticles in the same size (B). (C and D) Comparison of reflectance images of SiHa cells labeled with BSA/Au conjugated (C) and anti-EGFR gold conjugates (D). (E and F) Comparison of reflectance images of cervical biopsies labeled with anti-EGFR antibodies/gold nanoparticles conjugates for normal tissue (E) and abnormal tissue (F). Due to strong scattering from targeted gold nanoparticles, cancer cells and tissues can be differentiated from normal ones. All images were taken by a laser scanning confocal microscope in reflectance mode. (Reproduced with permission from Ref. [25].)

experience in optical engineering rendering them challenged for general researchers.

Due to the over-expressed EGFR on the cancer cell surface, anti-EGFR conjugated An NPs bind specifically to the cancer cells. As a result, the well-organized scattering pattern of the nanoparticles bound to the cancer cells could be clearly distinguished from the random distribution of the nanoparticles around the healthy cells (Fig. 6B). As the SPR of the nanoparticles is located around 540 nm on the cell monolayer, the nanoparticles scatter strongly in green-to-yellow color. In the following year [23], Huang et al. conjugated the anti-EGFR antibodies to gold nanorods via a poly (styrenesulfonate) linker and demonstrated that gold nanorod could also be used as imaging contrast agents for cancer cell diagnosis with a conventional optical microscope (Fig. 6C). Similar to gold nanospheres, the antibody-conjugated nanorods are specifically bound to the cancer cells, whereas they are randomly distributed in the case of normal cells. The SPR absorption at 800 nm gives the intense red color of the nanorods.

Spectroscopic cancer detection

The resonant surface plasmon oscillation can simply be visualized as a photon confined to the small nanoparticle size. This

strong confinement of the photon oscillation with the frequency of the light in resonance with SPR leads to a large increase of the electromagnetic field that decays within a distance comparable to the size of the nanoparticle [80]. In addition to enhance all the radiative properties such as absorption and scattering as we have discussed above, the field enhances the Raman scattering of adjacent molecules because the Raman intensity is directly proportional to the square of the field intensity imposed on the molecules [81]. This phenomenon is termed as surface enhanced Raman scattering (SERS). The induced field for the Raman enhancement is determined by the particle size, shape, composition and particle relative orientation and distance [82–87]. This indicates that for large Raman enhancement, asymmetric An NPs, which gives high curvature surface, are more favorable due to the “lightening-rod” effect. As demonstrated by Nikoobakht et al., enhancement factors on the order of 10^4 – 10^5 were observed for adsorbed molecules on the NRs while no such enhancement was observed on nanospheres under similar condition [88].

Recently, Huang et al. applied SERS by gold nanorods to diagnose cancer cells from normal cells [89] (Fig. 7). Gold nanorods are conjugated to anti-EGFR antibodies and then specifically bound to human oral cancer cells. Compared to HaCat normal cells, molecules including CTAB capping

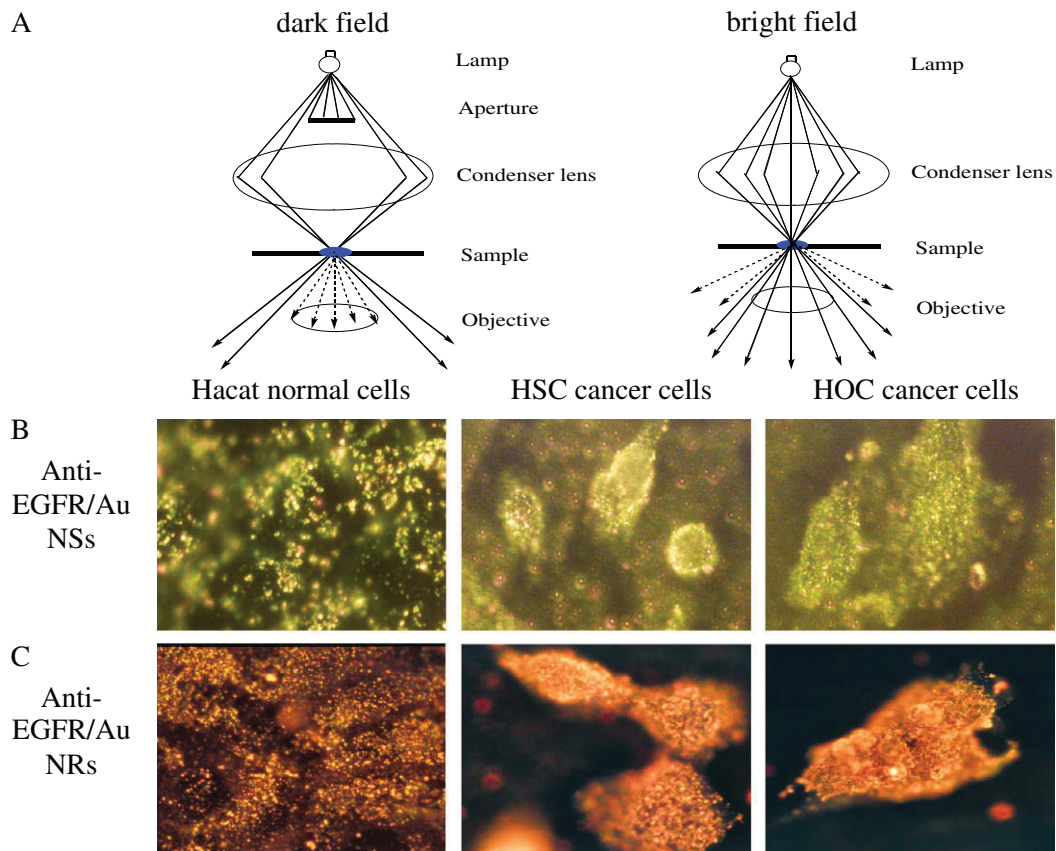


Figure 6 (A) Schematic illustration of dark field (left) and bright field (right) imaging; (B) Cancer cell diagnostics using dark field light scattering imaging of spherical gold nanoparticles; (C) Cancer cell diagnostics using dark field light scattering imaging of gold nanorods. The anti-EGFR-conjugated gold nanoparticles are bound to the cancer cells assembled in an organized fashion, while they are randomly distributed around normal cells, thus allowing for the optical differentiation and detection of the cancer cells. While gold nanoparticles show color in green due to SPR in visible region and gold nanorods show color in red due to SPR in NIR region ((B) is reproduced with permission from Ref. [28]. (D) is reproduced with permission from Ref. [23]).

molecules, PSS bridging molecules, the anti-EGFR antibodies as well as cellular components in the surface plasmon field of the gold nanorods on the cancer cell surface are found to give a Raman spectrum which is greatly enhanced due to the high surface plasmon field of aggregated nanorod assembly and sharp due to a homogenous environment. The polarization property of the SERS of the molecules monitored by the strongest band of the CTAB capping molecules (Fig. 7C and D) indicates that gold nanorods are assembled and aligned on the cancer cell surface and thus giving much stronger Raman enhancement. These observed properties can be used as molecular diagnostic signatures for cancer cells. Although traditional Raman has also been used to diagnose abnormal breast cancer tissue [90,91], SERS is more advantageous because it greatly enhances detection sensitivity and decreases signal acquisition time.

In addition to directly enhance the surrounding molecules to detect them, a Raman tag can be used as a spectroscopic imaging probe [92–94]. Raman tag is generally organic dye molecules with aromatic structures which has relative high Raman cross-sections. Its fluorescence is quenched when they are adsorbed on the metallic nanoparticles and thus Raman signals are able to be easily detected. For cancer diagnosis, the nanoparticles are physically adsorbed or chemically conju-

gated with both Raman tag and cancer targeting ligands. The report of the Raman fingerprints of the tag molecules indicates the binding of the nanoparticles to the cancer cells and thus identifies the targeted cells [95–98]. By conjugating different dye molecules on the same particles, multiplex detection can be achieved [99]. Recently, Nie and co-workers showed that SERS from tumor in mice can be obtained by using the Raman reporter adsorbed onto 60 nm spherical gold nanoparticles [95]. This study advanced the development of SERS from bench top to *in vivo* applications and offered possibility for future clinic intraoperative imaging based on Raman spectroscopic cancer detection.

Photothermal therapy (PTT)

Gold nanosphere-based PTT

Similar to scattering counterpart, Au NPs absorb light millions of times stronger than the organic dye molecules. Nearly 100% absorbed light is converted to heat via the nonradiative properties, as described above. As NPs are very photostable and biocompatible. These features make them a new generation photothermal contrast agents for photothermal therapy, in

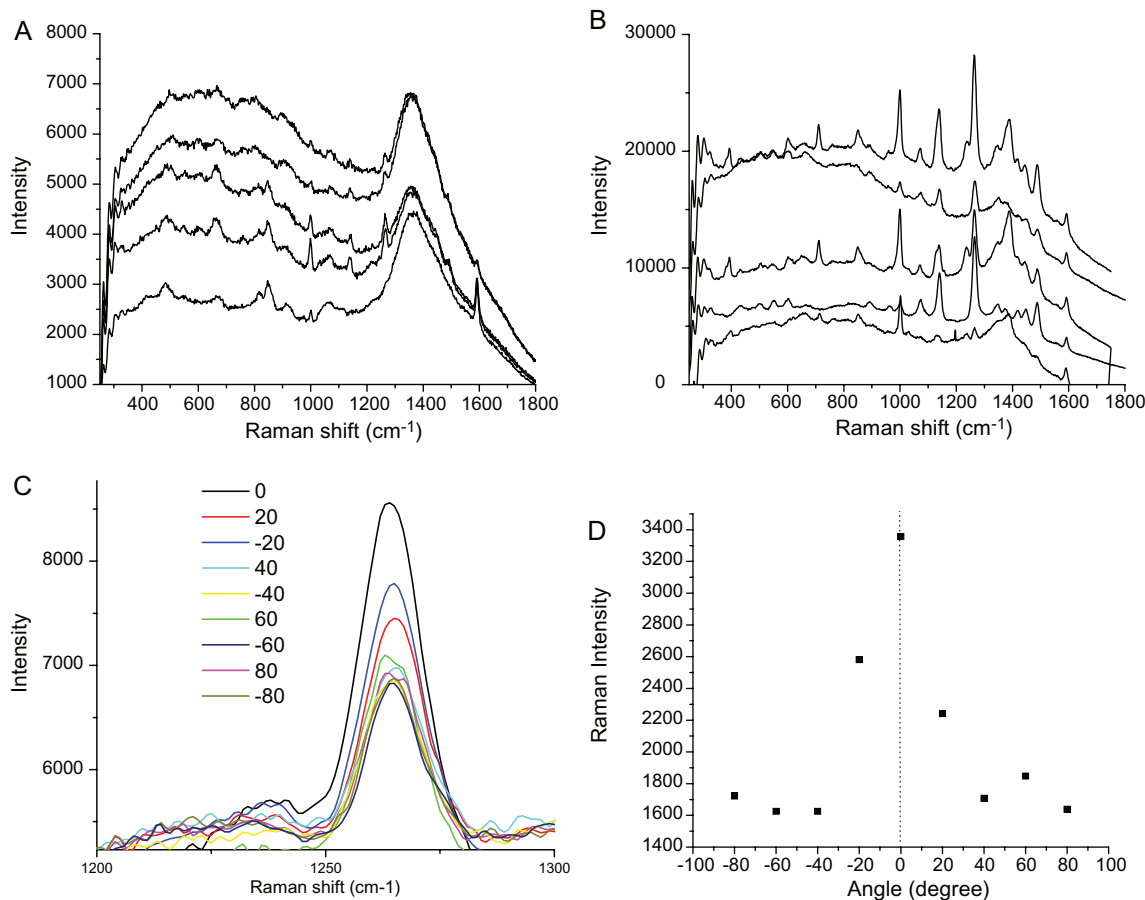


Figure 7 SERS of anti-EGFR antibody conjugated gold nanorods incubated with the HaCat normal cells (A) and HSC cancer cells (B). The polarized Raman spectra of the strong band at 1265 cm^{-1} of the gold nanorod capping molecules(CTAB) at different angles relative the electric field of the excitation laser (C) and the dependence of the Raman intensity of the 1265 cm^{-1} band on the angle (D). The angle is defined as the relative angle from the position at which CTAB shows the strongest intensity. The Raman spectra from the cancer cell samples are stronger, sharper, and polarized suggesting the potential of using surface enhanced Raman spectroscopy for the molecular-specific diagnosis of cancer. (Reproduced with permission from Ref. [89].)

which photon energy is converted to heat sufficient to induce cellular damage via thermal effects such as hyperthermia, coagulation and evaporation [100–102].

PTT using spherical gold nanoparticles [103–116] can be achieved with pulsed or cw visible lasers due to the SPR absorption in the visible region and thus such treatment is suitable for shallow cancer (e.g. skin cancer). The first thorough study using pulsed laser and gold nanospheres was performed in 2003 by Lin and co-workers for selective and highly localized photothermalysis of targeted lymphocytes cells [103]. Lymphocytes incubated with An NPs conjugated to antibodies were exposed to nanosecond laser pulses (Q-switched Nd:YAG laser, 565 nm wavelength, 20 ns duration) showed cell death with 100 laser pulses at an energy of 0.5 J/cm^2 . Adjacent cells just a few micrometers away without nanoparticles remained viable. Their numerical calculations showed that the peak temperature lasting for nanoseconds under a single pulse exceeds 2000 K at a fluence of 0.5 J/cm^2 with a heat fluid layer of 15 nm. The cell death is attributed mainly to the cavitation damage induced by the generated micro-scale bubbles around the nanoparticles. In the same year, Zharov et al. [104] performed similar studies on the photothermal destruc-

tion of K562 cancer cells. They further detected the laser induced-bubbles and studied their dynamics during the treatment using a pump-probe photothermal imaging technique. Later they demonstrated the technique *in vitro* on the treatment of some other type of cancer cells such as cervical and breast cancer using the laser induced-bubbles under nanosecond laser pulses [105–107]. Recent work has demonstrated the treatment modality for *in vivo* tumor ablation in a rat [115]. Intracellular bubble formation results in individual tumor cell damage.

The use of nanosecond pulsed laser for PTT is highly selective and localized damage controllable from few nanometers to tens of micrometers depending on the laser pulse duration and particle size [114]. This makes the method useful for single metastatic cell killing and small tumor eradication. However, the heating efficiency is relative low due to heat loss during the single pulse excitation. So the use of CW laser is favorable for effective heat accumulation to induce mild cell killing in a larger area mainly via hyperthermia and possible coagulation and vaporization depending on the heat content. Nonetheless, the treatment using CW lasers is time consuming (minutes) compared to pulsed laser (single pulse time). Examples using CW

lasers for PTT includes selective cancer cell killing [108] and targeted macrophage destruction [112]. In the study by El-Sayed et al. [108], 40 nm Au NPs were conjugated to anti-EGFR antibodies and targeted to two types of human head and neck cancer cells. Detected by dark field light scattering and surface plasmon absorption spectra on single cells, the nanoparticles induce cancer cell damage at 19 W/cm^2 after the irradiation with a Ar^+ laser at 514 nm for 4 min, while healthy cells do not show the loss of cell viability under the same treatment. Further numerical calculation shows temperature rises to 78°C capable of inducing cell damage [111].

Gold nanoshell-based PTT

For *in vivo* therapy of tumors under skin and deeply seated within tissue, NIR light is required because of its deep penetration due to minimal absorption of the hemoglobin and water molecules in tissues in this spectral region. Thus the nanoparticles have to be NIR active. In 2003, Hirsch et al. firstly demonstrated the NIR PTT both *in vitro* and *in vivo* using gold nanoshells [22]. Breast carcinoma cells incubated with PEGylated gold nanoshells, which possess tunable absorption in the NIR region as described in the previous sections, undergone irreversible photothermal damage after exposure to CW NIR light (diode laser, 820 nm, 35 W/cm^2) for 4 min, as indicated by the loss of Calcein AM staining (Fig. 8A) while cell treated with laser only did not show cell death (Fig. 8B). When

the nanoparticles were directly injected into tumor and then exposed to the same laser at intensity of 4 W/cm^2 for 4 min, magnetic resonance temperature imaging shows temperature rises over 30° leading to tissue damage, observed as coagulation, cell shrinkage, and loss of nuclear staining. In the following year, they injected the PEGylated nanoshells into blood stream of mice via tail vein [117]. The particles are accumulated into tumor via enhanced permeability and retention (EPR) effect [118–126]. This is because tumor vasculature is generally more leaky compared to normal vasculature due to rapid growth and thus nanoscale materials can be passively extravasated into the tumor interstitium. However, the lymphatic drainage system of the tumor tissue is impaired and thus the nanoparticles can not be excluded as wastes. So the nanoparticles are trapped in the tumor during their blood circulation. As shown in Fig. 8C, all tumors treated with both nanoparticles and laser underwent complete necrosis by day 10 without regrowth over 90 days (Fig. 8D). Followed work includes active targeting using antibodies and integrated imaging using light scattering properties [11,27,75,76,127–129].

Gold nanorod-based PTT

The blossoming of PTT in recent years are largely attributed to the emergence of gold nanorods. In 2006, El-Sayed et al. firstly demonstrated PTT using gold nanorods *in vitro* [23]. As detected by dark field imaging and micro-absorption spectra,

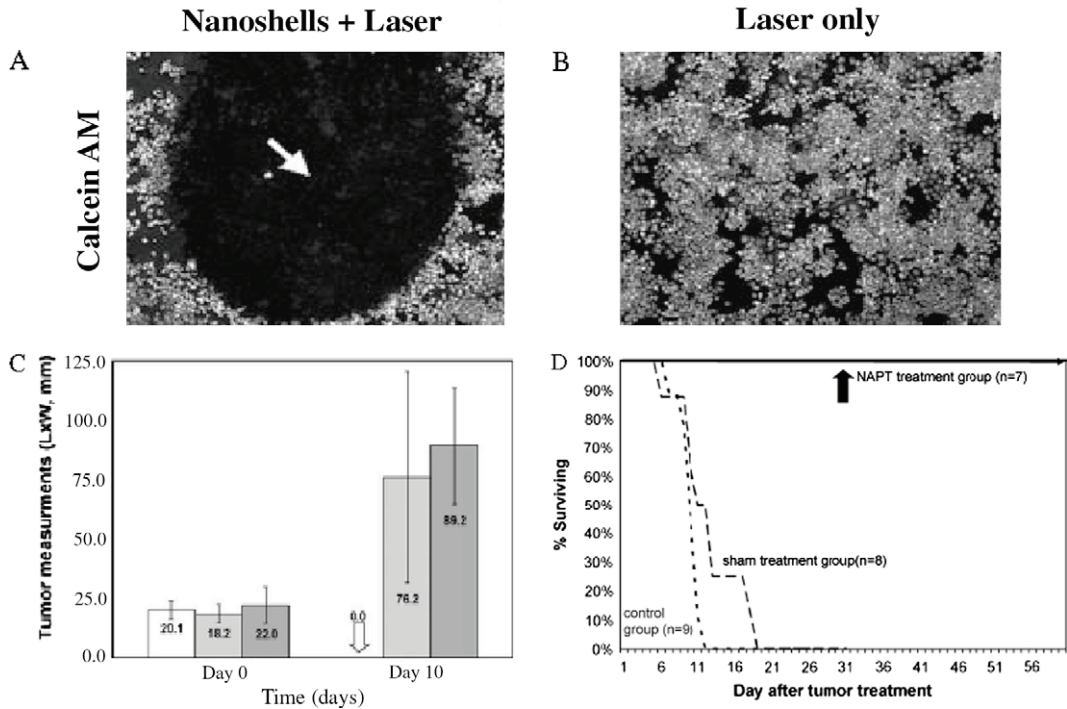


Figure 8 (A and B) Laser treatment ($820 \text{ nm}, 35 \text{ W/cm}^2$, 4 min) of Sk-BR-3 cells with (A) and without gold nanoshells (B). The loss of Calcein AM staining in B indicates photothermal destruction induced by gold nanoshells. (C) Tumor size comparison before and after photothermal treatment for different groups. Blank: nanoshell + laser; grey: sham treatment; dark grey: no nanoshells and no laser. At day 10, the laser + nanoshell treated tumors underwent complete necrosis while two control groups did not show the same results indicating the feasibility of gold nanoshells for photothermal tumor therapy. (D) Mice survival rate for different groups. Mice treated with both gold nanoshells and nanorods survive after 60 days of treatment ((A and B) are reproduced with permission from Ref. [22]. (C and D) are reproduced with permission from Ref. [117]).

the gold nanorods conjugated to anti-EGFR antibodies specifically bind to the ENT cancer cells (Fig. 6C). In the PTT treatment, a cw Ti:Sapphire laser at 800 nm, overlapping maximally with the SPR absorption band of the nanorods, was used for the electromagnetic irradiation of the cells labeled. Under laser exposure for 4 min, it was found that the cancer cells required half the laser energy (10 W/cm^2) to be photothermally damaged as compared to the normal cells (20 W/cm^2), attributed to the selective targeting of the over-expressed EGFR on the cancer cell surface by the anti-EGFR-conjugated gold nanorods (Fig. 9A) while the normal cells were not affected (Fig. 9B). Compared to nanoshells, the use

of gold nanorods enables effective treatment at three times lower laser intensity. This is because nanorods exhibit higher absorption efficiency than nanoshells with the SPR at the same wavelength [40]. In recent studies, it is been shown that when the linearly polarized light is converted into circularly polarized light, the light absorption by the gold nanorods are enhanced, which leads to ultra-low energy threshold for cancer killing (5 times lower) [130]. In the case of pulse laser irradiation, Niidome and co-workers found that it could induce cell death, but successive irradiation causes reshaping of the nanorods into nanospheres to prevent further cell death [131,132].

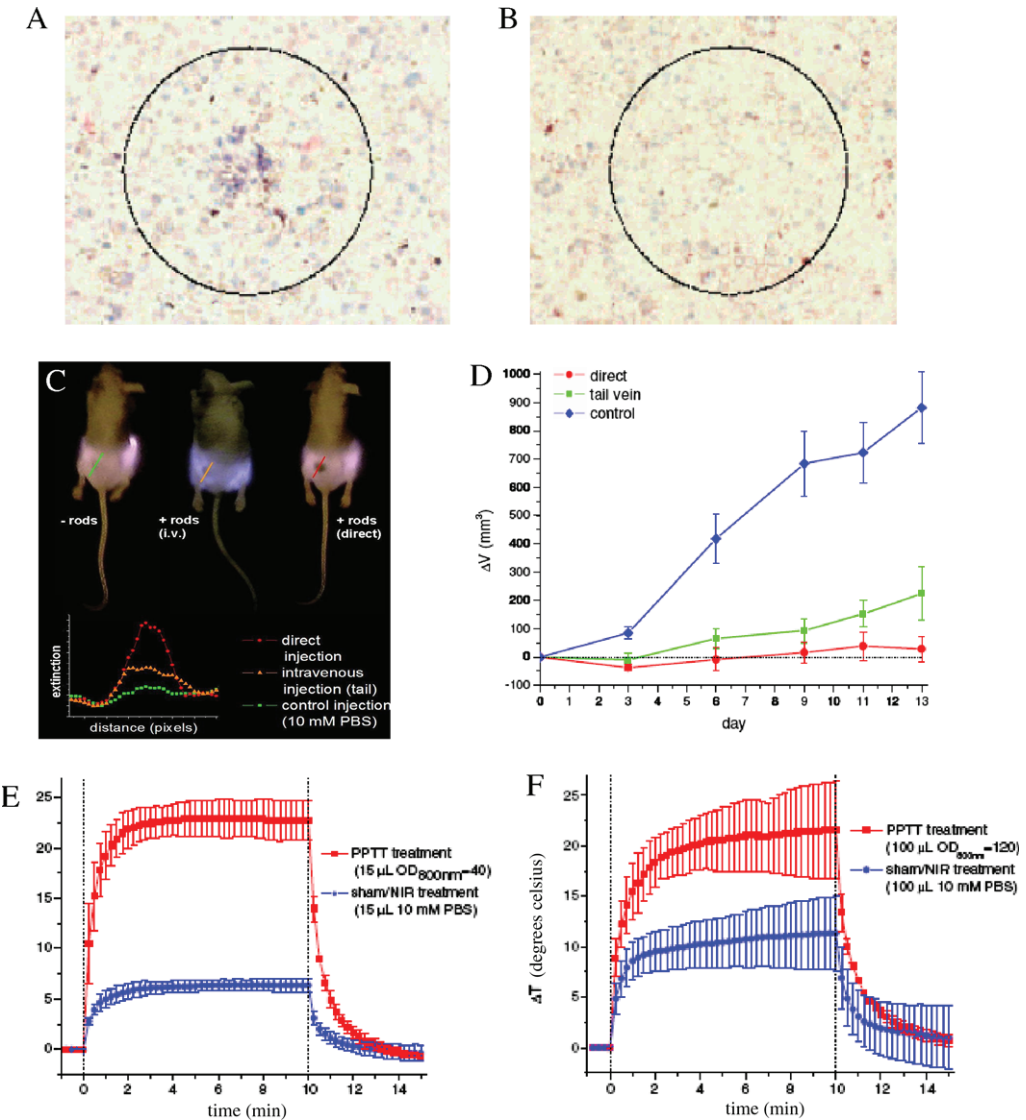


Figure 9 (A and B) Selective *in vitro* photothermal cancer therapy using gold nanorods. Under NIR laser treatment (800 nm, 10 W/cm^2 , 4 min), while the HSC-3 cancer cells undergo irreversible photodestruction indicated by trypan blue staining (A), the HaCat normal cells are not affected (B). (C) *In vivo* NIR tumor imaging and (D) *In vivo* photothermal tumor therapy using gold nanorods. The tumors are identified by a black spot under NIR illumination due to the light absorption by the nanorods that are administrated into the tumor either intratumorally or intravenously. NIR irradiation of the nanorod treated tumors leads to significant inhibition of the tumor growth rate compared to control tumors. (E and F) Temperature measurements during photothermal treatment with gold nanorods administrated by intratumoral injection (E) and intravenous injection (F). Both groups shown temperature rises over 20° capable of inducing tumor ablation ((A and B) are reproduced with permission from Ref. [23]. (C and F) are reproduced with permission from Ref. [137]).

Theoretical consideration for the photothermal heat generation has been carried out by Cortie and co-workers in their studies on the photothermal destruction of murine macrophage cells [133]. Based on a conductive heat transfer model, their results show that the effective temperature increases on the cells at a laser influence of 30 J/cm^2 is on the order of 10°C . This suggests heat-stress caused cell death instead of mechanical perforation of their membrane. Future studies by Wei and Cheng groups [134–136] show that the laser energy used to destroy the cells when the nanoparticles are located on the cytoplasm membrane is 10 times lower than that required when the nanoparticle are internalized inside the cytoplasm. The energy required for a fs laser is 10-fold lower than that by using a cw laser. Based on these results and staining of cell death pathways, they found that the cell death is initiated by the disruption of the plasma membrane. Subsequent influx of calcium ions induces membrane blebbing and damage of actin filaments. Obviously, apoptosis is the route of cell destruction by the laser heating of gold nanorods.

In the recent studies by El-Sayed et al. in a ENT cancer xenograft model [137], the nanorods are conjugated to mPEG-SH 5000 and injected into mice both intravenously and subcutaneously. Using the transmission imaging of the NIR laser with a customized camera, the tumor can be well identified due to the NIR light absorption by the nanorods in the tumor (Fig. 9C). The spectral profiling of the images clearly shows the difference of the delivery efficiency of gold nanorods by the two methods. After exposure to a cw NIR diode laser at 808 nm with intensity of $1\text{--}2\text{ W/cm}^2$ for 10 min, tumor growth is significantly inhibited for both treated groups (Fig. 9D). The intravenous treated tumors shows lower photothermal efficiency due to the less nanoparticles accumulated inside the tumor as shown in the NIR spectral imaging. Thermal transient measurements show that the temperature increased by over 20° sufficient to induce tumor destruction (Fig. 9E and F). Very recently, Bhatia and co-workers conducted similar studies on melanoma cancer xenograft [138]. The results show that single intravenous injection of PEGylated gold nanorods enables complete eradication of all irradiated tumors in mice without regrowth over 50-days of study time.

Gold nanocage-based PTT

Attempts using gold nanocages for PTT have also been made recently mainly by Xia and Li groups [12,24,139–142]. In the *in vitro* studies by Xia and co-workers, NIR femtosecond Ti:Sapphire pulsed laser was used to treat Sk-BR-3 breast cancer cells in the combination with HER-2 targeted 45 nm gold nanocages [24,140]. Quantitative characterization showed that under the exposure to the pulsed laser with energy of 6.4 W/cm^2 for 5 min, 55% cells underwent cellular damage [140]. In the *in vitro* studies by Li and co-workers, 30 nm gold nanocages are conjugated to anti-EGFR antibodies to target A431 cells [141]. At laser energy density of 40 W/cm^2 , almost all immunonanocage-treated cells were damaged, an effect not observed for all other control groups. *In vivo* biodistribution studies based on ^{111}In -labeled nanocages, they showed that anti-EGFR conjugated gold nanocages were delivered to EGFR-positive tumors at 6.8% ID/g. *Ex vivo* light scattering imaging

shows that nanocages are located to the preivasculature area of the tumor. Their further *in vivo* PTT of melanoma xenograft [143] showed successful photothermal ablation, as confirmed by positron emission tomography and histologic staining, using peptide-conjugated 43 nm gold nanocages after 24 h post treatment at energy dosage of 30 J/cm^2 .

Comparing all three classes of gold nanostructures for NIR PTT, gold nanorods have two significant advantages making them more feasible for future clinic settings: (1) Their synthetic procedure is relatively facile. The well established seed-mediated growth protocol enables production of gold nanorods of different aspect ratios with high yield and high quality within 2 h at RT [18]. In the case of nanoshells, it is very challenging to form a uniform shell on the silica core from the small gold clusters. To make nanocages, the preparation of silver nanocube precursors involves high temperature reaction (150°C) for over 20 h. (2) They possess superior long blood circulation time due to the anisotropic geometry. Recent studies have shown that PEGylated gold nanorods has a blood half-life time over 17 h in mice [138]. The elongated blood circulation time for rod-shaped nanoparticles compared to spheres has also been observed on other type of nanoparticles such as iron oxide nanoparticles [144]. In addition, the rod-shaped nanoparticles increase cellular affinity due to multiple ligand bindings [144].

Acknowledgment

X.H. would like to thank the distinguished CCNE postdoctoral fellowship at Emory-Georgia Tech Cancer Center for Nanotechnology Excellence and M.A.E. thanks the honor of Julius Brown Chair at Georgia Tech.

References

- [1] El-Sayed MA. Small is different: Shape-, size- and composition-dependent properties of some colloidal semiconductor nanocrystals. *Acc Chem Res* 2004;37(5):326–33.
- [2] El-Sayed MA. Some interesting properties of metals confined in time and nanometer space of different shapes. *Acc Chem Res* 2001;34(4):257–64.
- [3] Nie S, Xing Y, Kim GJ, Simons JW. Nanotechnology applications in cancer. *Annu Rev Biomed Eng* 2007;9: 257–88.
- [4] Link S, El-Sayed MA. Spectral properties and relaxation dynamics of surface plasmon electronic oscillations in gold and silver nanodots and nanorods. *J Phys Chem B* 1999;103(40):8410–26.
- [5] Link S, El-Sayed MA. Shape and size dependence of radiative, non-radiative and photothermal properties of gold nanocrystals. *Int Rev Phys Chem* 2000;19(3):409–53.
- [6] Link S, El-Sayed MA. Optical properties and ultrafast dynamics of metallic nanocrystals. *Annu Rev Phys Chem* 2003;54:331–66.
- [7] Huang X, Jain PK, El-Sayed IH, El-Sayed MA. Gold nanoparticles: interesting optical properties and recent applications in cancer diagnostics and therapy. *Nanomed* 2007;2(5):681–93.
- [8] Jain PK, Huang X, El-Sayed IH, El-Sayed MA. Review of some interesting surface plasmon resonance-enhanced properties of noble metal nanoparticles and their applications to biosystems. *Plasmonics* 2007;2(3):107–18.

- [9] Huang X, Jain PK, El-Sayed IH, El-Sayed MA. Plasmonic photothermal therapy (PPTT) using gold nanoparticles. *Lasers Med Sci* 2008;23(3):217–28.
- [10] Jain PK, Huang X, El-Sayed IH, El-Sayed MA. Noble metals on the nanoscale: optical and photothermal properties and some applications in imaging, sensing, biology and medicine. *Acc Chem Res* 2008;41(12):1578–86.
- [11] Lal S, Clare SE, Halas NJ. Nanoshell-enabled photothermal cancer therapy: impending clinical impact. *Acc Chem Res* 2008;41(12):1842–51.
- [12] Skrabalak SE, Chen J, Sun Y, Lu X, Au L, Cobley CM, et al. Gold nanocages: synthesis, properties and applications. *Acc Chem Res* 2008;41(12):1587–95.
- [13] Frens G. Controlled nucleation for the regulation of the particle size in monodisperse gold suspensions. *Nat Phys Sci* 1973;241:20–2.
- [14] Turkevich J, Stevenson PC, Hillier J. A study of the nucleation and growth processes in the synthesis of colloidal gold. *Disc Farad Soc* 1951;11:55–75.
- [15] Turkevich J, Garton G, Stevenson PC. The color of colloidal gold. *J Colloid Sci* 1954;9(Suppl 1):26–35.
- [16] Xia Y, Halas NJ. Shape-controlled synthesis and surface plasmonic properties of metallic nanostructures. *MRS Bull* 2005;30(5):338–43.
- [17] Yu YY, Chang SS, Lee CL, Wang CRC. Gold nanorods: electrochemical synthesis and optical properties. *J Phys Chem B* 1997;101(34):6661–4.
- [18] Nikoobakht B, El-Sayed MA. Preparation and growth mechanism of gold nanorods (NRs) using seed-mediated growth method. *Chem Mater* 2003;15(10):1957–62.
- [19] Murphy CJ, Sau TK, Gole AM, Orendorff CJ, Gao J, Gou L, et al. Anisotropic metal nanoparticles: synthesis, assembly and optical applications. *J Phys Chem B* 2005;109(29):13857–70.
- [20] Oldenburg SJ, Averitt RD, Westcott SL, Halas NJ. Nanoengineering of optical resonances. *Chem Phys Lett* 1998;288(2–4):243–7.
- [21] Sun Y, Mayers BT, Xia Y. Template-engaged replacement reaction: a one-step approach to the large-scale synthesis of metal nanostructures with hollow interiors. *Nano Lett* 2002;2(5):481–5.
- [22] Hirsch LR, Stafford RJ, Bankson JA, Sershen SR, Rivera B, Price RE, et al. Nanoshell-mediated near-infrared thermal therapy of tumors under magnetic resonance guidance. *Proc Natl Acad Sci USA* 2003;100(23):13549–54.
- [23] Huang X, El-Sayed IH, Qian W, El-Sayed MA. Cancer cell imaging and photothermal therapy in the near-infrared region by using gold nanorods. *J Am Chem Soc* 2006;128(6): 2115–20.
- [24] Chen J, Wang D, Xi J, Au L, Siekkinen A, Warsen A, et al. Immuno gold nanocages with tailored optical properties for targeted photothermal destruction of cancer cells. *Nano Lett* 2007;7(5):1318–22.
- [25] Sokolov K, Follen M, Aaron J, Pavlova I, Malpica A, Lotan R, et al. Real-time vital optical imaging of precancer using anti-epidermal growth factor receptor antibodies conjugated to gold nanoparticles. *Cancer Res* 2003;63(9):1999–2004.
- [26] Sokolov K, Aaron J, Hsu B, Nida D, Gillenwater A, Follen M, et al. Optical systems for *in vivo* molecular imaging of cancer. *Technol Cancer Res Treat* 2003;2(6):491–504.
- [27] Loo C, Lin A, Hirsch L, Lee MH, Barton J, Halas N, et al. Nanoshell-enabled photonics-based imaging and therapy of cancer. *Technol Cancer Res Treat* 2004;3(1):33–40.
- [28] El-Sayed IH, Huang X, El-Sayed MA. Surface plasmon resonance scattering and absorption of anti-EGFR antibody conjugated gold nanoparticles in cancer diagnostics: applications in oral cancer. *Nano Lett* 2005;5(5):829–34.
- [29] Mie G. A contribution to the optics of turbid media, especially colloidal metallic suspensions. *Ann Phys* 1908;25:377–445.
- [30] Kerker M. The scattering of light and other electromagnetic radiation. New York: Academic Press; 1969.
- [31] Papavassiliou GC. Optical properties of small inorganic and organic metal particles. *Prog Solid State Chem* 1979;12:185–271.
- [32] Bohren CF, Huffman DR. Absorption and scattering of light by small particles. New York: Wiley; 1983.
- [33] Kreibig U, Vollmer M. Optical properties of metal clusters. Springer; 1995.
- [34] Liz-Marzán LM. Nanometals: Formation and color. *Mater Today* 2004;7(2):26–31.
- [35] Faraday M. Preparation of colloidal gold. *Philos Trans* 1857;147:145–81.
- [36] Creighton JA, Eadon DG. Ultraviolet-visible absorption spectra of the colloidal metallic elements. *J Chem Soc Farad Trans* 1991;87(24):3881–91.
- [37] Link S, El-Sayed MA. Size and temperature dependence of the plasmon absorption of colloidal gold nanoparticles. *J Phys Chem B* 1999;103(21):4212–7.
- [38] Kreibig U, von Fragstein C. The limitation of electron mean free path in small silver particles. *Z Phys* 1969;224:307–23.
- [39] Kreibig U. *Z Phys* 1970;234:307.
- [40] Jain PK, Lee KS, El-Sayed IH, El-Sayed MA. Calculated absorption and scattering properties of gold nanoparticles of different size, shape, and composition: applications in biological imaging and biomedicine. *J Phys Chem B* 2006;110(14):7238–48.
- [41] Lee KS, El-Sayed MA. Dependence of the enhanced optical scattering efficiency relative to that of absorption for gold metal nanorods on aspect ratio, size, end-cap shape and medium refractive index. *J Phys Chem B* 2005;109(43):20331–8.
- [42] Gans R. Form of ultramicroscopic particles of silver. *Ann Phys* 1915;47:270–84.
- [43] Liu M, Guyot-Sionnest P. Mechanism of silver(I)-assisted growth of gold nanorods and bipyramids. *J Phys Chem B* 2005;109(47):22192–200.
- [44] Link S, Mohamed MB, El-Sayed MA. Simulation of the optical absorption spectra of gold nanorods as a function of their aspect ratio and the effect of the medium dielectric constant. *J Phys Chem B* 1999;103(16):3073–7.
- [45] Link S, El-Sayed MA. Erratum: Simulation of the optical absorption spectra of gold nanorods as a function of their aspect ratio and the effect of the medium dielectric constant (*Journal of Physical Chemistry B* (1999) 103B). *J Phys Chem B* 2005;109(20):10531–2.
- [46] Purcell EM, Pennypacker CP. Scattering and absorption of light by nonspherical dielectric grains. *Astrophys J* 1973;186:705–14.
- [47] Draine BT. The discrete-dipole approximation and its application to interstellar graphite grains. *Astrophys J* 1988;333:848–72.
- [48] Draine BT, Goodman J. Beyond Clausius–Mossotti: wave propagation on a polarizable point lattice and the discrete dipole approximation. *Astrophys J* 1993;405(2):685–97.
- [49] Draine BT, Flatau PJ. Discrete-dipole approximation for scattering calculations. *J Opt Soc Am A: Opt Image Sci Vis* 1994;11(4):1491–9.
- [50] Draine BT. The discrete-dipole approximation for light scattering by irregular targets. In: Mishchenko MI, Hovenier JW, Travis LD, editors. Light scattering by nonspherical particles: theory, measurement and applications. San Diego: Academic Press; 2000. p. 131.
- [51] Lee KS, El-Sayed MA. Gold and silver nanoparticles in sensing and imaging: sensitivity of plasmon response to size, shape and metal composition. *J Phys Chem B* 2006;110(39):19220–5.
- [52] Prodan E, Radloff C, Halas NJ, Nordlander P. A hybridization model for the plasmon response of complex nanostructures. *Science* 2003;302(5644):419–22.

- [53] Jain PK, El-Sayed MA. Universal scaling of plasmon coupling in metal nanostructures: extension from particle pairs to nanoshells. *Nano Lett* 2007;7(9):2854–8.
- [54] Chen J, Saeki F, Wiley BJ, Cang H, Cobb MJ, Li ZY, et al. Gold nanocages: bioconjugation and their potential use as optical imaging contrast agents. *Nano Lett* 2005;5(3):473–7.
- [55] Chen J, Wiley B, Li ZY, Campbell D, Saeki F, Cang H, et al. Gold nanocages: engineering their structure for biomedical applications. *Adv Mater* 2005;17(18):2255–61.
- [56] Link S, Burda C, Wang ZL, El-Sayed MA. Electron dynamics in gold and gold–silver alloy nanoparticles: the influence of a nonequilibrium electron distribution and the size dependence of the electron–phonon relaxation. *J Chem Phys* 1999;111(3):1255–64.
- [57] Link S, Burda C, Mohamed MB, Nikoobakht B, El-Sayed MA. Femtosecond transient-absorption dynamics of colloidal gold nanorods: shape independence of the electron–phonon relaxation time. *Phys Rev B – Condens Mat Mater Phys* 2000;61(9):6086–90.
- [58] Mohamed MB, Ahmadi TS, Link S, Braun M, El-Sayed MA. Hot electron and phonon dynamics of gold nanoparticles embedded in a gel matrix. *Chem Phys Lett* 2001;343(1–2):55–63.
- [59] Link S, Furube A, Mohamed MB, Asahi T, Masuhara H, El-Sayed MA. Hot electron relaxation dynamics of gold nanoparticles embedded in $MgSO_4$ powder compared to solution: the effect of the surrounding medium. *J Phys Chem B* 2002;106(5):945–55.
- [60] Link S, Hathcock DJ, Nikoobakht B, El-Sayed MA. Medium effect on the electron cooling dynamics in gold nanorods and truncated tetrahedra. *Adv Mater* 2003;15(5):393–6.
- [61] Link S, Burda C, Mohamed MB, Nikoobakht B, El-Sayed MA. Laser photothermal melting and fragmentation of gold nanorods: energy and laser pulse-width dependence. *J Phys Chem A* 1999;103(9):1165–70.
- [62] Link S, Burda C, Nikoobakht B, El-Sayed MA. Laser-induced shape changes of colloidal gold nanorods using femtosecond and nanosecond laser pulses. *J Phys Chem B* 2000;104(26):6152–63.
- [63] Yguerabide J, Yguerabide EE. Light-scattering submicroscopic particles as highly fluorescent analogs, their use as tracer labels in clinical, biological applications I. Theory. *Anal Biochem* 1998;262(2):137–56.
- [64] Yguerabide J, Yguerabide EE. Light-scattering submicroscopic particles as highly fluorescent analogs, their use as tracer labels in clinical, biological applications II. Experimental characterization. *Anal Biochem* 1998;262(2):157–76.
- [65] Sönnichsen C, Franzl T, Wilk T, Von Plessen G, Feldmann J, Wilson O, et al. Drastic reduction of plasmon damping in gold nanorods. *Phys Rev Lett* 2002;88(7):774021–4.
- [66] Asian K, Lakowicz JR, Geddes CD. Nanogold plasmon resonance-based glucose sensing. 2. Wavelength-ratiometric resonance light scattering. *Anal Chem* 2005;77(7):2007–14.
- [67] Orendorff CJ, Sau TK, Murphy CJ. Shape-dependent plasmon-resonant gold nanoparticles. *Small* 2006;2(5):636–9.
- [68] Zhu J, Huang L, Zhao J, Wang Y, Zhao Y, Hao L, et al. Shape dependent resonance light scattering properties of gold nanorods. *Mater Sci Eng B – Solid-State Mater Adv Technol* 2005;121(3):199–203.
- [69] Raub CB, Orwin EJ, Haskell R. Immunogold labeling to enhance contrast in optical coherence microscopy of tissue engineered corneal constructs. *Ann Int Conf IEEE Eng Med Biol* 2004;2:1210–3.
- [70] Aaron JS, Oh J, Larson TA, Kumar S, Milner TE, Sokolov KV. Increased optical contrast in imaging of epidermal growth factor receptor using magnetically actuated hybrid gold/iron oxide nanoparticles. *Opt Express* 2006;14(26):12930–43.
- [71] Oyelere AK, Chen PC, Huang X, El-Sayed IH, El-Sayed MA. Peptide-conjugated gold nanorods for nuclear targeting. *Bioconjugate Chem* 2007;18(5):1490–7.
- [72] Yguerabide J, Yguerabide EE. Resonance light scattering particles as ultrasensitive labels for detection of analytes in a wide range of applications. *J Cell Biochem Suppl* 2001;37:71–81.
- [73] Raschke G, Kowarik S, Franzl T, Sönnichsen C, Klar TA, Feldmann J, et al. Biomolecular recognition based on single gold nanoparticle light scattering. *Nano Lett* 2003;3(7):935–8.
- [74] Kumar S, Harrison N, Richards-Kortum R, Sokolov K. Plasmonic nanosensors for imaging intracellular biomarkers in live cells. *Nano Lett* 2007;7(5):1338–43.
- [75] Loo C, Lowery A, Halas N, West J, Drezek R. Immunotargeted nanoshells for integrated cancer imaging and therapy. *Nano Lett* 2005;5(4):709–11.
- [76] Loo C, Hirsch L, Lee MH, Chang E, West J, Halas N, et al. Gold nanoshell bioconjugates for molecular imaging in living cells. *Opt Lett* 2005;30(9):1012–4.
- [77] Ding H, Yong KT, Roy I, Pudavar HE, Law WC, Bergey EJ, et al. Gold nanorods coated with multilayer polyelectrolyte as contrast agents for multimodal imaging. *J Phys Chem C* 2007;111(34):12552–7.
- [78] Oldenburg AL, Hansen MN, Zweifel DA, Wei A, Boppart SA. Plasmon-resonant gold nanorods as low backscattering albedo contrast agents for optical coherence tomography. *Opt Express* 2006;14(15):6724–38.
- [79] Zsigmondy R. Colloids and the ultramicroscope: a manual of colloid chemistry and ultramicroscopy. 2nd ed. John Wiley and Sons; 1914.
- [80] Jain PK, Huang W, El-Sayed MA. On the universal scaling behavior of the distance decay of plasmon coupling in metal nanoparticle pairs: a plasmon ruler equation. *Nano Lett* 2007;7(7):2080–8.
- [81] Kneipp K, Kneipp H, Itzkan I, Dasari RR, Feld MS. Surface-enhanced Raman scattering and biophysics. *J Phys Condens Mater* 2002;14(18):R597–624.
- [82] Krug JT, Wang GD, Emory SR, Nie S. Efficient Raman enhancement and intermittent light emission observed in single gold nanocrystals. *J Am Chem Soc* 1999;121(39):9208–14.
- [83] Hao E, Schatz GC. Electromagnetic fields around silver nanoparticles and dimers. *J Chem Phys* 2004;120(1):357–66.
- [84] Hao E, Schatz GC, Hupp JT. Synthesis and optical properties of anisotropic metal nanoparticles. *J Fluor* 2004;14(4):331–41.
- [85] Gluodenis M, Foss CA. The effect of mutual orientation on the spectra of metal nanoparticle rod–rod and rod–sphere pairs. *J Phys Chem B* 2002;106(37):9484–9.
- [86] Jain PK, Eustis S, El-Sayed MA. Plasmon coupling in nanorod assemblies: optical absorption, discrete dipole approximation simulation and exciton-coupling model. *J Phys Chem B* 2006;110(37):18243–53.
- [87] Cotton TM, Kim JH, Chumanov GD. Application of surface-enhanced Raman spectroscopy to biological systems. *J Raman Spectrosc* 1991;22:729–42.
- [88] Nikoobakht B, Wang J, El-Sayed MA. Surface-enhanced Raman scattering of molecules adsorbed on gold nanorods: off-surface plasmon resonance condition. *Chem Phys Lett* 2002;366(1–2):17–23.
- [89] Huang X, El-Sayed IH, Qian W, El-Sayed MA. Cancer cells assemble and align gold nanorods conjugated to antibodies to produce highly enhanced, sharp and polarized surface Raman spectra: a potential cancer diagnostic marker. *Nano Lett* 2007;7(6):1591–7.
- [90] Haka AS, Shafer-Peltier KE, Fitzmaurice M, Crowe J, Dasari RR, Feld MS. Identifying microcalcifications in benign and malignant breast lesions by probing differences in their

- chemical composition using Raman spectroscopy. *Cancer Res* 2002;62(18):5375–80.
- [91] Haka AS, Shafer-Peltier KE, Fitzmaurice M, Crowe J, Dasari RR, Feld MS. Diagnosing breast cancer by using Raman spectroscopy. *Proc Natl Acad Sci USA* 2005;102(35):12371–6.
- [92] Cao YC, Jin R, Mirkin CA. Nanoparticles with Raman spectroscopic fingerprints for DNA and RNA detection. *Science* 2002;297(5586):1536–15340.
- [93] Keren S, Zavaleta C, Cheng Z, De La Zerda A, Gheysens O, Gambhir SS. Noninvasive molecular imaging of small living subjects using Raman spectroscopy. *Proc Natl Acad Sci USA* 2008;105(15):5844–9.
- [94] Gong JL, Jiang JH, Yang HF, Shen GL, Yu RQ, Ozaki Y. Novel dye-embedded core-shell nanoparticles as surface-enhanced Raman scattering tags for immunoassay. *Anal Chim Acta* 2006;564(2):151–7.
- [95] Qian X, Peng XH, Ansari DO, Yin-Goen Q, Chen GZ, Shin DM, et al. *In vivo* tumor targeting and spectroscopic detection with surface-enhanced Raman nanoparticle tags. *Nat Biotechnol* 2008;26(1):83–90.
- [96] Kim JH, Kim JS, Choi H, Lee SM, Jun BH, Yu KN, et al. Nanoparticle probes with surface enhanced Raman spectroscopic tags for cellular cancer targeting. *Anal Chem* 2006;78(19):6967–73.
- [97] Lee S, Chon H, Lee M, Choo J, Shin SY, Lee YH, et al. Surface-enhanced Raman scattering imaging of HER2 cancer markers overexpressed in single MCF7 cells using antibody conjugated hollow gold nanospheres. *Biosens Bioelectron* 2009;24(7):2260–3.
- [98] Lee S, Kim S, Choo J, Soon YS, Lee YH, Ha YC, et al. Biological imaging of HEK293 cells expressing PLC γ 1 using surface-enhanced Raman microscopy. *Anal Chem* 2007;79(3):916–22.
- [99] Schlücker S, Kömpe K, Gellner M. Multiplexing with SERS labels using mixed SAMs of Raman reporter molecules. *Anal Bioanal Chem* 2009;394(7):1839–44.
- [100] Svaasand LO, Gomer CJ, Morinelli E. On the physical rationale of laser induced hyperthermia. *Lasers Med Sci* 1990;5(2):121–7.
- [101] Goldman L. Biomedical aspects of the laser. Berlin: Springer-Verlag; 1967.
- [102] Goldman L, Rockwell Jr RJ. Laser systems and their applications in medicine and biology. *Adv Biomed Eng Med Phys* 1968;1:317–82.
- [103] Pitsillides CM, Joe EK, Wei X, Anderson RR, Lin CP. Selective cell targeting with light-absorbing microparticles and nanoparticles. *Biophys J* 2003;84(6):4023–32.
- [104] Zharov VP, Galitovsky V, Viegas M. Photothermal detection of local thermal effects during selective nanophotothermolysis. *Appl Phys Lett* 2003;83(24):4897–9.
- [105] Zharov VP, Galitovskaya E, Viegas M. Photothermal guidance for selective photothermolysis with nanoparticles. *Proc SPIE – Int Soc Opt Eng* 2004;5319:291–300.
- [106] Zharov VP, Galitovskaya EN, Johnson C, Kelly T. Synergistic enhancement of selective nanophotothermolysis with gold nanoclusters: potential for cancer therapy. *Lasers Surg Med* 2005;37(3):219–26.
- [107] Zharov VP, Kim JW, Curiel DT, Everts M. Self-assembling nanoclusters in living systems: application for integrated photothermal nanodiagnostics and nanotherapy. *Nanomed Nanotechnol Biol Med* 2005;1(4):326–45.
- [108] El-Sayed IH, Huang X, El-Sayed MA. Selective laser photothermal therapy of epithelial carcinoma using anti-EGFR antibody conjugated gold nanoparticles. *Cancer Lett* 2006;239(1):129–35.
- [109] Khlebtsov B, Zharov V, Melnikov A, Tuchin V, Khlebtsov N. Optical amplification of photothermal therapy with gold nanoparticles and nanoclusters. *Nanotechnology* 2006;17(20):5167–579.
- [110] Pissuwan D, Valenzuela SM, Cortie MB. Therapeutic possibilities of plasmonically heated gold nanoparticles. *Trends Biotechnol* 2006;24(2):62–7.
- [111] Huang X, Jain PK, El-Sayed IH, El-Sayed MA. Determination of the minimum temperature required for selective photothermal destruction of cancer cells with the use of immunotargeted gold nanoparticles. *Photochem Photobiol* 2006;82(2):412–7.
- [112] Pissuwan D, Cortie CH, Valenzuela SM, Cortie MB. Gold nanosphere-antibody conjugates for hyperthermal therapeutic applications. *Gold Bull* 2007;40(2):121–9.
- [113] Huang X, Qian W, El-Sayed IH, El-Sayed MA. The potential use of the enhanced nonlinear properties of gold nanospheres in photothermal cancer therapy. *Lasers Surg Med* 2007;39(9):747–53.
- [114] Pustovalov VK, Smetannikov AS, Zharov VP. Photothermal and accompanied phenomena of selective nanophotothermolysis with gold nanoparticles and laser pulses. *Laser Phys Lett* 2008;5(11):775–92.
- [115] Hleb EY, Hafner JH, Myers JN, Hanna EY, Rostro BC, Zhdanok SA, et al. LANTCET: elimination of solid tumor cells with photothermal bubbles generated around clusters of gold nanoparticles. *Nanomed* 2008;3(5):647–67.
- [116] Liu X, Lloyd MC, Fedorenko IV, Bapat P, Zhukov T, Huo Q. Enhanced imaging and accelerated photothermalysis of A549 human lung cancer cells by gold nanospheres. *Nanomed* 2008;3(5):617–26.
- [117] O’Neal DP, Hirsch LR, Halas NJ, Payne JD, West JL. Photothermal tumor ablation in mice using near infrared-absorbing nanoparticles. *Cancer Lett* 2004;209(2):171–6.
- [118] Kreuter J. Drug targeting with nanoparticles. *Eur J Drug Metabol Pharm* 1994;19(3):253–6.
- [119] Kwon GS, Kataoka K. Block copolymer micelles as long-circulating drug vehicles. *Adv Drug Del Rev* 1995;16(2–3):295–309.
- [120] Langer R. Drug delivery and targeting. *Nature* 1998;392(6679 Suppl):5–10.
- [121] Müller RH, Mäder K, Gohla S. Solid lipid nanoparticles (SLN) for controlled drug delivery – a review of the state of the art. *Eur J Pharm Biopharm* 2000;50(1):161–77.
- [122] Pillai O, Panchagnula R. Polymers in drug delivery. *Curr Opin Chem Biol* 2001;5(4):447–51.
- [123] Sershen S, West J. Implantable, polymeric systems for modulated drug delivery. *Adv Drug Del Rev* 2002;54(9):1225–35.
- [124] Hillaireau H, Couvreur P. Polymeric nanoparticles as drug carriers. In: Uchegbu IF, editor. *Polymers in drug delivery*. Boca Raton, FL, USA: CRC Press; 2006. p. 101–10.
- [125] Uchegbu IF. Pharmaceutical nanotechnology: polymeric vesicles for drug and gene delivery. *Expert Opin Drug Del* 2006;3(5):629–40.
- [126] Moghimi SM, Vega E, Garcia ML, Al-Hanbali OAR, Rutt KJ. Polymeric nanoparticles as drug carriers and controlled release implant devices. In: Torchilin VP, editor. *Nanoparticulates as drug carriers*. London: Imperial College Press; 2006. p. 29–42.
- [127] Lowery AR, Gobin AM, Day ES, Halas NJ, West JL. Immunonanoshells for targeted photothermal ablation of tumor cells. *Int J Nanomed* 2006;1(2):149–54.
- [128] Gobin AM, Lee MH, Halas NJ, James WD, Drezek RA, West JL. Near-infrared resonant nanoshells for combined optical imaging and photothermal cancer therapy. *Nano Lett* 2007;7(7):1929–34.
- [129] Diagradjane P, Shetty A, Wang JC, Elliott AM, Schwartz J, Shentu S, et al. Modulation of *in vivo* tumor radiation response via gold nanoshell-mediated vascular-focused hyperthermia:

- characterizing an integrated antihypoxic and localized vascular disrupting targeting strategy. *Nano Lett* 2008;8(5):1492–500.
- [130] Li JA, Day D, Gu M. Ultra-low energy threshold for cancer photothermal therapy using transferrin-conjugated gold nanorods. *Adv Mater* 2008;20(20):3866–71.
- [131] Takahashi H, Niidome T, Nariai A, Niidome Y, Yamada S. Gold nanorod-sensitized cell death: microscopic observation of single living cells irradiated by pulsed near-infrared laser light in the presence of gold nanorods. *Chem Lett* 2006;35(5):500–1.
- [132] Takahashi H, Niidome T, Nariai A, Niidome Y, Yamada S. Photothermal reshaping of gold nanorods prevents further cell death. *Nanotechnology* 2006;17(17):4431–5.
- [133] Pissuwan D, Valenzuela SM, Killingsworth MC, Xu X, Cortie MB. Targeted destruction of murine macrophage cells with bioconjugated gold nanorods. *J Nanoparticle Res* 2007;9(6):1109–24.
- [134] Huff TB, Tong L, Zhao Y, Hansen MN, Cheng JX, Wei A. Hyperthermic effects of gold nanorods on tumor cells. *Nanomed* 2007;2(1):125–32.
- [135] Tong L, Zhao Y, Huff TB, Hansen MN, Wei A, Cheng JX. Gold nanorods mediate tumor cell death by compromising membrane integrity. *Adv Mater* 2007;19(20):3136–41.
- [136] Tong L, Cheng JX. Gold nanorod-mediated photothermolysis induces apoptosis of macrophages via damage of mitochondria. *Nanomed* 2009;4(3):265–76.
- [137] Dickerson EB, Dreaden EC, Huang X, El-Sayed IH, Chu H, Pushpanketh S, et al. Gold nanorod assisted near-infrared plasmonic photothermal therapy (PPTT) of squamous cell carcinoma in mice. *Cancer Lett* 2008;269(1):57–66.
- [138] Von Maltzahn G, Park JH, Agrawal A, Bandaru NK, Das SK, Sailor MJ, et al. Computationally guided photothermal tumor therapy using long-circulating gold nanorod antennas. *Cancer Res* 2009;69(9):3892–900.
- [139] Skrabalak SE, Chen J, Au L, Lu X, Li X, Xia Y. Gold nanocages for biomedical applications. *Adv Mater* 2007;19(20):3177–84.
- [140] Au L, Zheng D, Zhou F, Li ZY, Li X, Xia Y. A quantitative study on the photothermal effect of immuno gold nanocages targeted to breast cancer cells. *ACS Nano* 2008;2(8):1645–52.
- [141] Melancon MP, Lu W, Yang Z, Zhang R, Cheng Z, Elliot AM, et al. *In vitro* and *in vivo* targeting of hollow gold nanoshells directed at epidermal growth factor receptor for photothermal ablation therapy. *Mol Cancer Therap* 2008;7(6):1730–9.
- [142] Lim YT, Cho MY, Choi BS, Noh YW, Chung BH. Diagnosis and therapy of macrophage cells using dextran-coated near-infrared responsive hollow-type gold nanoparticles. *Nanotechnology* 2008;19(37):375105.
- [143] Lu W, Xiong C, Zhang G, Huang Q, Zhang R, Zhang JZ, et al. Targeted photothermal ablation of murine melanomas with melanocyte-stimulating hormone analog-conjugated hollow gold nanospheres. *Clin Cancer Res* 2009;15(3):876–86.
- [144] Park JH, Von Maltzahn G, Zhang L, Schwartz MP, Ruoslahti E, Bhatia SN, et al. Magnetic iron oxide nanoworms for tumor targeting and imaging. *Adv Mater* 2008;20(9):1630–5.